Power Electronics and Drives
Volume 7(42), 2022 DOI: 10.2478/pead-2022-0012

sciendo

Power Electronics and Drives

Sliding Mode Control-Based MPPT and Output Voltage Regulation of a Stand-alone PV System

Research paper

Nelson Luis Manuel*, Nihat İnanç

Kırıkkale University, Kırıkkale, Turkey

Received: June 28, 2022; Accepted: July 30, 2022

Abstract: When it comes to reducing emissions caused by the generation of electricity, among different renewable energy sources, the solar energy gains prominence, due to its geographical availability, simplicity of implementation, and absence of physical moving parts. However, the performance of photovoltaic systems is dependent on environmental conditions. Depending on temperature and solar irradiation, the photovoltaic (PV) system has an operating point where maximum power can be generated. The techniques that are implemented to find this operating point are the so-called maximum power point tracking (MPPT) algorithms. Since weather conditions are variable in nature, the output voltage of the PV system needs to be regulated to remain equal to the reference. Most of the existing studies focus either on MPPT or on voltage regulation of the PV system. In this paper, the two-stage PV system is implemented so that both MPPT and voltage regulation are achieved simultaneously. Additionally, an improved version of the perturb and observe (P&O) algorithm based on artificial potential fields (APF), called APF-P&O, is presented. According to the results of the simulations carried out in MATLAB/Simulink software, the APF-P&O method is more efficient than the conventional method.

Keywords: *sliding mode control • PV systems • MPPT • APF-P&O • voltage regulation*

1. Introduction

In order to ensure a sustainable future, many countries have been devising various strategies. In the context of energy systems, one of these strategies is the reduction or replacement of electricity generation based on non-renewable energies through the implementation of energy generation systems based on sources that are environmentally friendly (Ullah, 2021). Solar energy, among other forms of renewable energy, has been gaining both scientific and industrial interest in recent years due to its wide availability (Ma et al., 2020). The application of photovoltaic systems in distributed generation and direct current (DC) microgrids, not to mention the development of power electronics technology, further extend the facets of research on solar energy. However, the efficiency of a photovoltaic system is highly dependent on environmental conditions. Furthermore, for the generated power to be of high quality, the voltage delivered by the PV system needs to be regulated. Therefore, to increase the efficiency of the photovoltaic system and guarantee high quality of the energy produced, it is necessary to implement strategies to track the point of maximum power and regulate the output voltage.

State-of-the-art studies and comparison of different methods for maximum power point tracking (MPPT) are carried out in many studies (Podder et al., 2019; Kermadi et al., 2020; Sarvi and Azadian, 2021). Among different techniques, perturb and observe (P&O) and incremental conductance (InC) are commonly used for MPPT due to their easy implementation (Chowdhury et al., 2021; Grzesiak, 2017). Some variants of these algorithms have been reported to improve the settling time and reduce output power fluctuations of the PV system. In order to overcome the drawbacks of conventional P&O, an adaptive P&O method based on the Manhattan metric distance is proposed

* *Email: nelsonluismanuel@gmail.com*

in Kesilmiş (2022). An MPPT technique is proposed in Sheikh Ahmadi et al. (2022), where the InC method is used to improve the convergence speed, and the particle swarm optimisation (PSO) algorithm is used to reduce ripples in the output power of a PV system. A hybrid technique for MPPT that combines a modified version of P&O and the chimp optimisation algorithm (ChOA) is proposed in Elahi et al. (2022). The Owl search algorithm is used together with the InC method to reduce the convergence time to the maximum power point (MPP) and mitigate the inherent limitations of the conventional InC method in Altamimi et al. (2021). An improved version of the InC and integral regulator (IR) is used to track the peak output power of a PV system interfaced by a DC–DC boost converter in Stephen et al. (2022). In Pradhan et al. (2022), the roach infestation (RI) algorithm is presented for the MPPT of a photovoltaic system, and fuzzy logic is used to generate variable step sizes for the InC method in Ali et al. (2021). Different approaches to voltage regulation can also be found in the literature, including the classic proportional–integral–derivative (PID) control (Park and Cho, 2014), feedback linearisation (Sulligoi et al., 2014), fuzzy logic control (Jayaprakash and Ramakrishnan, 2014), model predictive control (Wei et al., 2017), and sliding mode control (Benadli et al., 2021; Ling et al., 2018), among others. Sliding mode control (SMC) has been reported as a convenient technique for controlling the voltage of DC–DC converters since its operating structure is inherently commutative (Utkin, 2013).

Many of the studies presented in the literature separately address the maximum power tracking and voltage regulation strategies for PV systems, instead of dealing with both at the same time (Mira et al., 2013). However, for the delivered power to have a high quality and to improve the efficiency of the photovoltaic system, both the MPPT and voltage regulation are aspects that must be considered simultaneously. To satisfy both objectives, the two-stage conversion topology is employed to control the photovoltaic system (Ravindranath Tagore et al., 2022). Therefore, in this paper, the two-stage PV system control for MPPT and voltage regulation is presented. In the first stage, the boost converter is used, and an improved version of P&O is proposed to find the PV voltage corresponding to the MPP. The reference voltage found by the P&O serves as an input to the sliding mode controller, which then sends the necessary control signals to the boost converter so that maximum power is generated. In the second stage, the buck converter is used for voltage regulation, and its control is done by applying the sliding mode controller. In this manner, MPPT and voltage regulation issues are simultaneously addressed.

2. Structure of the Photovoltaic System

The structure of a photovoltaic system can be separated into two essential parts: the photovoltaic module and the conversion subsystem (Ma et al., 2020). The PV system studied in this paper is based on the two-stage conversion topology, as illustrated in Figure 1. The first DC–DC converter is a step-up (or boost) and the second one is a step-down (or buck) converter. The boost converter is used to modify the output impedance seen from the photovoltaic module terminals so that the point of intersection between the I–V characteristic curve of the PV module and the load line matches the point of maximum power that can be delivered under the given environmental conditions.

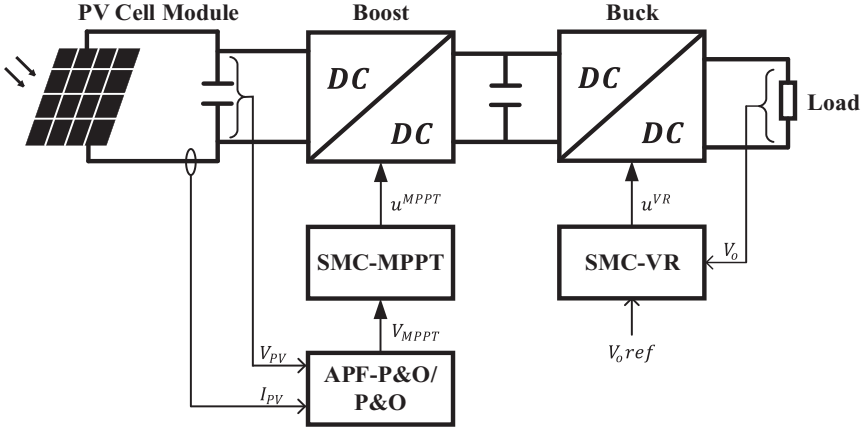

Fig. 1. Schematic of the applied control strategy for the two-stage PV system. APF, artificial potential fields; MPPT, maximum power point tracking; P&O, perturb and observe.

In the second stage, the stability of the voltage supplied to the loads is achieved through the control of the step-down converter.

2.1. Electrical circuit of a photovoltaic cell

The photovoltaic cell is considered as the basic constituent of a PV module (Mohamed and Abd El Sattar, 2019). The PV cells are electrically connected in series and/or parallel to achieve the voltage, current, and power levels for which the module is designed (Saidi and Benachaiba, 2016). The power delivered by the photovoltaic generator is dependent on the ambient temperature and solar irradiation. Generally, to model the behaviour of a photovoltaic cell, an electrical circuit composed of a current source (I_{ph}), a diode (D), a series resistance (R_s), and a parallel resistance (R_{sh}) is considered. The resistance R_{sh} is connected in parallel with an inverted diode D to express nonlinearity and losses due to leakage currents, and resistance R_s is used to model voltage drops when the module is connected to load (Mohamed and Abd El Sattar, 2019). The electrical circuit of a photovoltaic cell is shown in Figure 2.

Applying Kirchoff's current law to the electrical circuit of the single-diode photovoltaic cell model, the expression of the output current of the PV cell can be found as shown in Eq. (1).

$$I = I_{ph} - I_D - I_{sh} \tag{1}$$

where I is the output current of the PV cell, I_{ph} is the photogenerated current, I_D is the current through the diode, and I_{sh} is the current through the resistor R_{sh}.

The expression to determine the current flowing through the diode, also known as a Shockley equation, can be computed using Eq. (2) (Kordestani et al., 2018).

$$I_D = I_o \left\{ \exp\left[\frac{q\left(V + IR_s\right)}{AkT} \right] - 1 \right\} \tag{2}$$

Therefore, the equation of the PV cell output current can be rewritten as in Eq. (3).

$$I = I_{ph} - I_o \left\{ \exp\left[\frac{q\left(V + IR_s\right)}{AkT} \right] - 1 \right\} - \frac{\left(V + IR_s\right)}{R_{sh}} \tag{3}$$

where I_o is the saturation current, q is the electron charge ($q = 1.60 \times 10^{-19}$ C), k is the Boltzmann constant ($k = 1.38 \times 10^{-23}$ J / K), T is the operating temperature of the cell, and A is the idealisation constant of the diode D.

The photogenerated current is dependent on temperature and solar irradiation. It is defined as demonstrated in Eq. (4).

$$I_{ph} = \left[Iscn + k_i\left(T - T_n\right) \right] \frac{G}{G_n} \tag{4}$$

where I_{scn} denotes the short-circuit current under the standard test conditions (STC) ($T_n = 25\,^{\circ}\text{C}$ and $G_n = 1{,}000$ W / m^2), T is the ambient temperature, T_n is the nominal temperature, G and G_n are the actual and nominal irradiations, respectively, and k_i is the temperature coefficient of the short-circuit current.

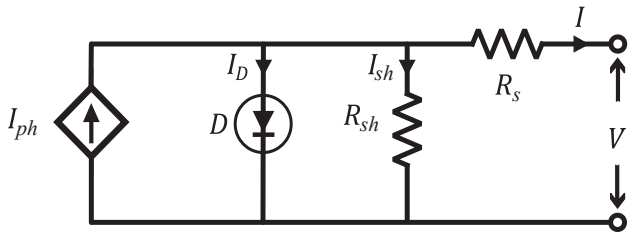

Fig. 2. Electrical circuit of a single diode PV cell.

The saturation current of the photovoltaic cell is mathematically defined by Eq. (5).

$$I_o = I_{rr}\left(\frac{T}{T_n}\right)^3 \exp\left[\frac{qE_g}{kA}\left(\frac{1}{T_n}-\frac{1}{T}\right)\right] \tag{5}$$

where I_{rr} is the reverse saturation current at temperature T_n and solar irradiation G_n and E_g is the band gap energy of the silicon PV cell ($E_g = 1.10$ eV). The rest of the parameters remain with the same definitions.

For a photovoltaic module composed of N_s PV cells in series and N_p PV cells in parallel, the output current is given by Eq. (6) (Farhat et al., 2017).

$$I = N_p I_{ph} - N_p I_o \left\{\exp\left[\frac{q\left(N_s V + \left(N_s/N_p\right)IR_s\right)}{N_s AkT}\right] - 1\right\} - \frac{N_s V + \left(N_s/N_p\right)IR_s}{\left(N_s/N_p\right)R_{sh}} \tag{6}$$

2.2. State-space averaged models of the DC–DC converters

In this subsection, the models of the DC–DC converters, which are part of the conversion circuit of the photovoltaic system under study, are presented. The DC–DC boost converter is used in the first stage of the conversion. This converter, in addition to boosting the output voltage of the solar panel, is used to ensure that the power extracted from the PV module is the maximum possible by switching (ON and OFF) the input signal of the transistor Q at high frequencies. In Figure 3, the boost converter circuit is shown.

Considering the continuous conduction mode (CCM) of operation and choosing the current through the inductor and the voltage across the capacitor as the state variables, the averaged model of the boost converter can be defined by Eqs (7) and (8) (Farhat et al., 2017; Rahman Habib et al., 2019).

$$\frac{di_L(t)}{dt} = -(1-u)\frac{1}{L}v_C(t) + \frac{1}{L}v_{in} \tag{7}$$

$$\frac{dv_C(t)}{dt} = (1-u)\frac{1}{C}i_L(t) - \frac{1}{RC}v_C(t) \tag{8}$$

where i_L denotes the current through the inductor ($i_L = i_{in}$), v_C is the voltage across the capacitor ($v_C = v_o$), and u is the control signal ($u \in \{0,1\}$). In the boost converter circuit, the parameters R, L, and C represent the load resistance, the input circuit inductance, and the output filter capacitance, respectively, and v_{in} is the supply voltage of the step-up converter.

For the second stage of conversion, the DC–DC buck converter is considered. Here, the buck converter is used to step down and stabilise the voltage delivered to the load. In Figure 4, the circuit of the buck-type DC–DC converter is shown.

Considering that during the operation of the buck converter the average value of the current passing through the inductor does not reach zero and adopting the current in the inductor and the capacitor voltage as the state variables, the averaged model of the buck converter is mathematically summarised by Eqs (9) and (10).

$$\frac{di_L(t)}{dt} = -\frac{1}{L}v_C(t) + \frac{u}{L}v_{in} \tag{9}$$

$$\frac{dv_C(t)}{dt} = \frac{1}{C}i_L(t) - \frac{1}{RC}v_C(t) \tag{10}$$

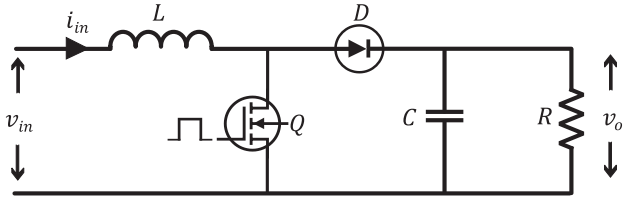

Fig. 3. Circuit of a DC–DC boost converter.

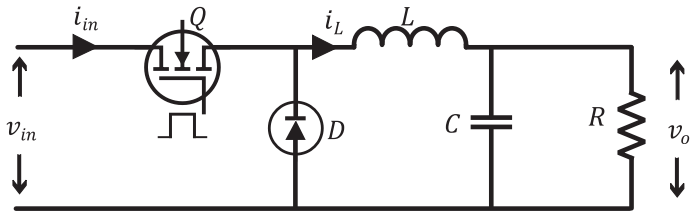

Fig. 4. Circuit of a DC–DC buck converter.

where i_L is the current through the inductor, v_C is the voltage across the capacitor ($v_C = v_o$), and u is the control signal ($u \in \{0,1\}$). In the buck converter circuit, the parameters R, L, and C represent the load resistance, the circuit inductance, and the output filter capacitance, respectively, and v_{in} is the supply voltage of the step-down converter.

3. Control Strategy for MPPT

In order to get the best out of the solar generation system, tracking the MPP is crucial. There are several methods for MPPT. Among the different methods, P&O is one of the most popular due to its simplicity (Farhat et al., 2017). Furthermore, in the P&O method, prior knowledge of the characteristics of the photovoltaic module is not required (Saidi and Benachaiba, 2016). The operation of the P&O method is based on perturbing the output voltage of the PV module and observing the resultant output power. If the actual value of the measured power $P(k)$ is greater than its previously obtained value $P(k-1)$, then the direction of the perturbation is maintained; otherwise, the movement of the perturbation is done in the opposite direction (Kordestani et al., 2018).

In Figure 5, the flowchart that summarises the operation of the P&O algorithm is depicted. As shown in the flowchart, the algorithm begins by sensing the values of voltage $V(k)$ and current $I(k)$ to compute the power $P(k)$ generated by the PV system. Then, the difference between the actual voltage value and its previous value $V(k-1)$ is computed and saved in the variable ΔV. The difference between the actual value of the measured power and its previous value $P(k-1)$ is also calculated, and the result is recorded in the variable ΔP. Afterwards, the output voltage V of the photovoltaic system is perturbed (increases or decreases) depending on the ΔP and ΔV signals. The amount of increase or decrease of the output voltage is defined by the value ΔD. The value ΔD is chosen based on tests and simulations (Farhat et al., 2017). If very small ΔD values are chosen, the system becomes slow to find the MPP; on the other hand, very large ΔD values can result in loss of information creating high levels of ripple in the generated power. Therefore, the trade-off between the time of convergence to the MPP and the steady-state ripple levels of the generated power must be considered when defining the value of ΔD.

3.1. Proposal for improvement of the conventional P&O method

In this subsection, a proposal to improve the conventional P&O method is presented. The improvement is based on artificial potential fields (APF), hereinafter also referred to as APF-P&O. The proposed method, besides being simple to implement, has no computational complexity. Its implementation is done by adding just a few lines of code to the original method and only depends on the output voltage of the photovoltaic module (which is already an input of the conventional P&O method), i.e., the proposed APF-P&O method does not increase the number of input variables of the conventional method. In APF, the target point or desired region is modelled as a point or zone with an attractive potential field that pulls the controlled states towards the desired point or region (Manuel et al., 2021). Assuming that the minimum and maximum values of expected solar irradiation and the respective voltage values at the point of maximum power are known, a zone of attraction that contains all points of maximum power for the range of expected solar irradiation can be defined, as shown in Figure 6. The idea is to produce attractive forces so that the output voltages of the PV module remain in the attraction zone, which is the zone where the MPPs are located.

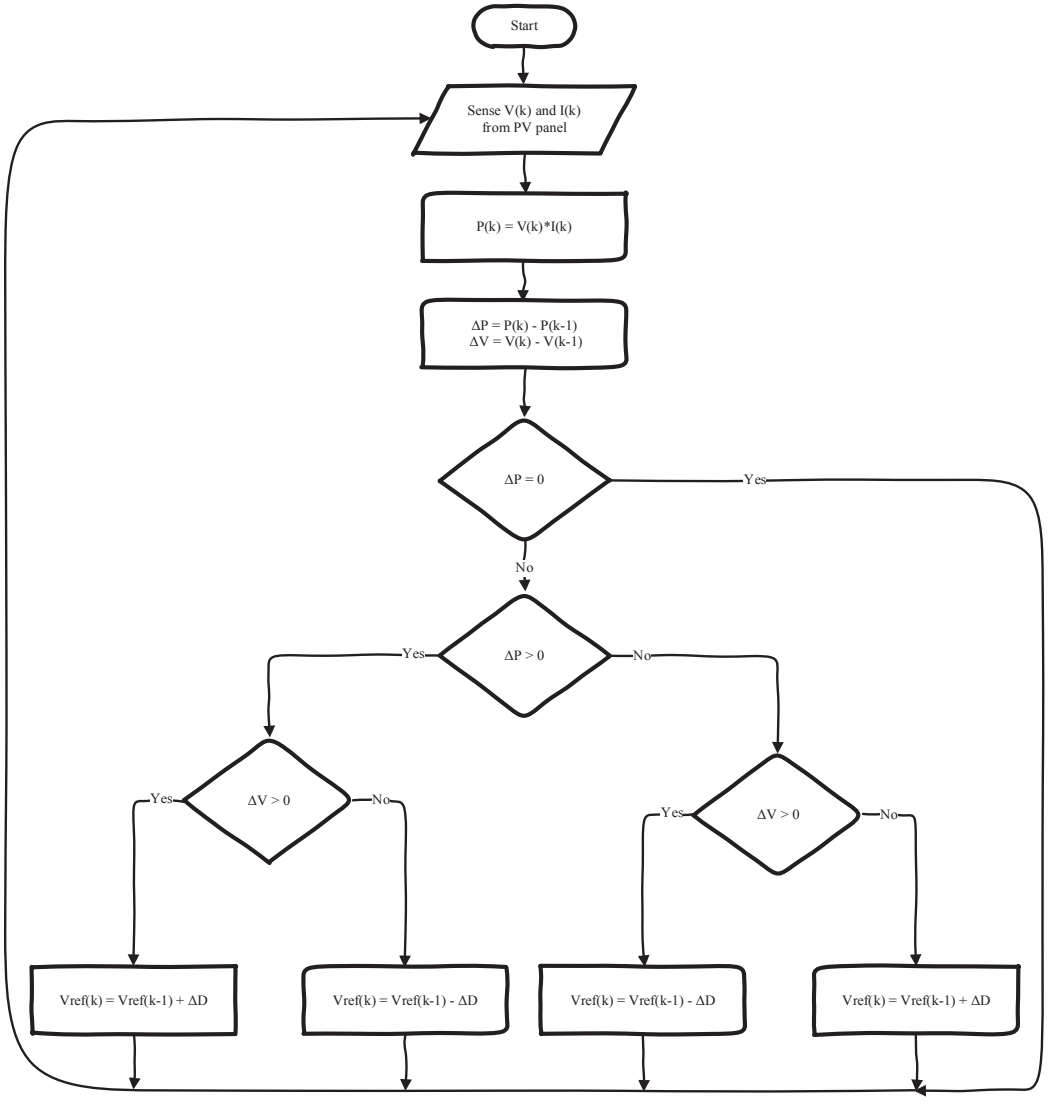

Fig. 5. Flowchart showing the operation of the P&O method. P&O, perturb and observe.

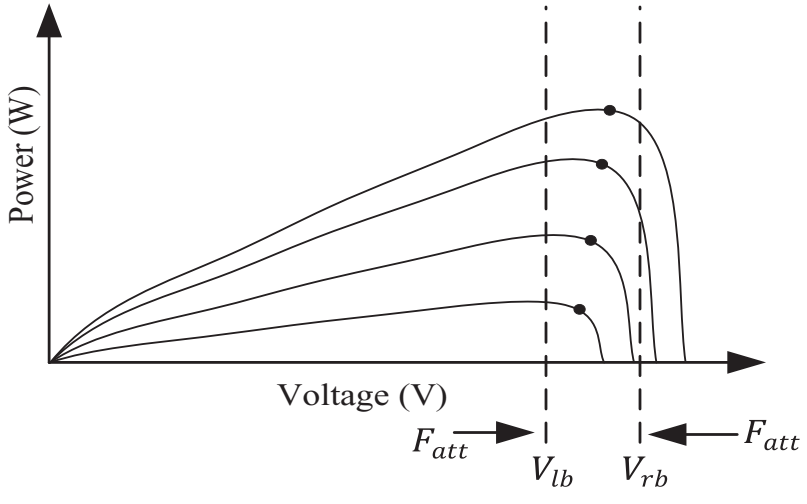

Fig. 6. Principle of the presented APF-P&O method. APF, artificial potential fields; P&O, perturb and observe.

The attractive potential field can be defined according to Eq. (11), where $U_{att}\left(V_{PV}\right)$ denotes the attractive potential field, K_{att} is a positive design parameter, V_{PV} is the output voltage of the PV module, and V_{lb} and V_{rb} are the left and right boundary voltages of the attraction zone, respectively.

$$U_{att}(\mathrm{V}_{PV}) = \begin{cases} \frac{1}{2}K_{att}\left(V_{PV} - V_{lb}\right)^2, & \mathrm{V}_{PV} < \mathrm{V}_{lb} \\ \frac{1}{2}K_{att}\left(V_{PV} - V_{rb}\right)^2, & \mathrm{V}_{PV} > \mathrm{V}_{rb} \end{cases} \tag{11}$$

Applying the negative gradient to the attractive field expression, the corresponding attractive force is obtained, as shown in Eq. (12).

$$F_{att} = -\nabla(U_{att}) = \begin{cases} K_{att}(\mathrm{V}_{lb} - \mathrm{V}_{PV}), & \mathrm{V}_{PV} < \mathrm{V}_{lb} \\ K_{att}(\mathrm{V}_{rb} - \mathrm{V}_{PV}), & \mathrm{V}_{PV} > \mathrm{V}_{rb} \end{cases} \tag{12}$$

where F_{att} is the resultant force of attraction. The law to determine the step size (ΔD) for the proposed APF-P&O algorithm is established according to Eq. (13).

$$\Delta D = \begin{cases} \chi, & V_{lb} \le V_{PV} \le V_{rb} \\ F_{att}, & otherwise \end{cases} \tag{13}$$

where χ is a relatively small positive design parameter that represents the step size when the algorithm is in the attraction zone. The value of χ is set small to reduce steady-state power fluctuations. For χ, a typical value of 0.001 was chosen (Saidi et al., 2019; Xu et al., 2015). The positive design parameter (K_{att}) makes it possible to manipulate the degree of influence of the attractive force (F_{att}). Depending on the type of application, K_{att} can be defined to be a constant or a variable, as long as the condition of being a positive value is met. A negative K_{att} value would cause the voltage to diverge from the MPP. In this paper, after different tests, K_{att} equal to 1 is used. If $K_{att} << 1$, the speed of convergence of the reference voltage to the attraction zone decreases, while if $K_{att} >> 1$, the probability of the reference voltage escaping from the attraction zone increases. As can be understood, while the voltage generated by the PV system is outside the attraction zone, the algorithm generates forces of attraction necessary to bring the voltage to the zone where the MPPs are located, and thus, the convergence speed is increased.

3.2. Sliding mode controller for MPPT

The voltage at the MPP (V_{MPP}) estimated by the P&O method or by the proposed APF-P&O serves as a reference for the SMC. The implemented SMC will produce the necessary control signals to make the output voltage of the PV module equal to the reference voltage, thus reaching the MPP. Assuming the error (e) as the difference between the PV module output voltage (V_{PV}) and the reference voltage (V_{MPP}), a sliding surface s can be defined as in Eq. (14).

$$s = e = V_{PV} - V_{MPP} \tag{14}$$

The control law u to achieve the MPPT can be defined as in Eq. (15).

$$u = \frac{1}{2}\left[1 + sign(\mathrm{s})\right] \tag{15}$$

A rigorous stability analysis is presented in Section 3 of the paper (Farhat et al., 2017), where it is proved that, in fact, by applying this control strategy, the system stability conditions at the MPP of the PV module interfaced with a boost converter are satisfied.

4. Control Strategy for Output Voltage Regulation

In this section, our attention is devoted to the strategy applied for the regulation of the output voltage of the photovoltaic system. SMC has been recognised as one of the powerful control strategies for power converters (Komurcugil et al., 2021). SMC is a robust non-linear control technique, which uses a discontinuous control action that switches between two different system structures, in such a manner that a new system motion, known as sliding mode, is achieved on a surface (or manifold) previously designed for this end (Wu et al., 2022). This characteristic of switching between different structures of the system makes the SMC a convenient control technique to be applied in DC–DC power converters, which are switching devices by their nature (Utkin, 2013). For these reasons, the SMC is chosen for the regulation of the output voltage of the PV system. In the following subsections, details about the technique used are presented.

One of the important features of the sliding mode control is its low sensitivity to system parameter variations (Inomoto et al., 2022). This is possible by employing a high-switching control law, which forces the system trajectories to converge in a predetermined zone within the state space and to remain in this zone thereafter. In SMC parlance, this zone is denoted as a sliding surface. Considering the buck converter state-space model presented earlier, the sliding surface is defined as in Eq. (16) (Goudarzian et al., 2019).

$$\sigma(x) = x_1 - x_1^*; \;\; x_1^* = \mu_1\left(x_2 - x_2^*\right) + \mu_2 \int \left(x_2 - x_2^*\right) \tag{16}$$

where $\sigma(x)$ is the sliding surface, x_1 is the current through the inductor, x_2 denotes the voltage across the capacitor, μ_1 and μ_2 are design parameters, x_1^* is the desired current, x_2^* is the desired voltage, and R denotes load resistance. The control objective is to make the output voltage x_2 of the PV system equal to the desired voltage x_2^*. This problem can also be redefined in terms of the current through the inductor, i.e., a control law u should be found such that the current x_1 is equal to its reference value x_1^*. If this occurs, then the difference $\Delta x_2 = x_2^* - x_2$, which leads to $\Delta \dot{x}_2 = -(1/RC)\Delta x_2$, will tend to zero over time (Utkin, 2013). In this paper, the cascade control structure of the SMC is adopted, where the inner loop current reference is obtained from the outer loop voltage control using a linear controller (Wu et al., 2022). In order to drive the system state variables to the sliding surface ($\sigma = 0$), the control law u presented in Eq. (17) is generally employed (Utkin, 2013).

$$u = \frac{1}{2}\left[1 - sign(\sigma)\right] \tag{17}$$

The stability analysis of the system applying the defined control law can be done using Lyapunov's theory. In Eq. (18), the Lyapunov function $V(\sigma)$ that will be considered to evaluate the stability is presented:

$$V(\sigma) = \frac{1}{2}\sigma^2 \tag{18}$$

For the system to be considered stable, the selected Lyapunov function has to meet the following conditions (Inomoto et al., 2022):

a) $V(\sigma) > 0$;
b) $V(\sigma) = 0 \Leftrightarrow \sigma = 0$;
c) $\dot{V}(\sigma) = \sigma\dot{\sigma} < 0$.

It is simple to conclude that the first two conditions are fulfilled by the selected function, except for the third condition which deserves demonstration. This third condition is also known as the reaching condition in the sliding mode control literature. Computing the derivative of the sliding surface presented in Eq. (16), Eq. (19) is obtained.

$$\dot{\sigma} = \dot{x}_1 = \left(\frac{v_{in}}{L}u - \frac{1}{L}x_2\right) \tag{19}$$

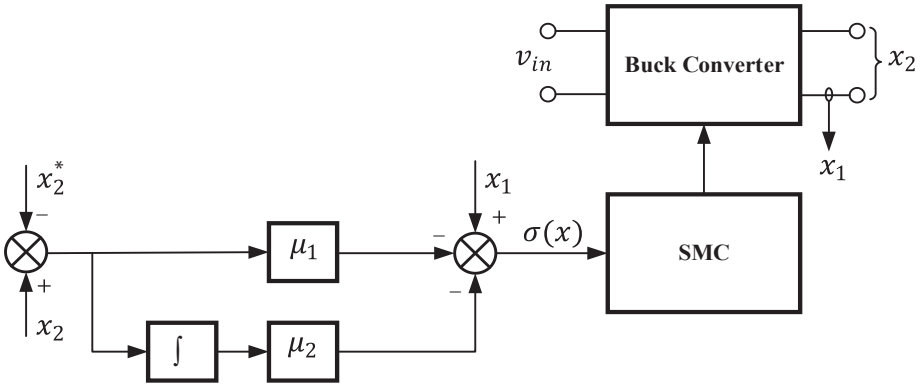

Fig. 7. Scheme for regulating the output voltage of the PV system.

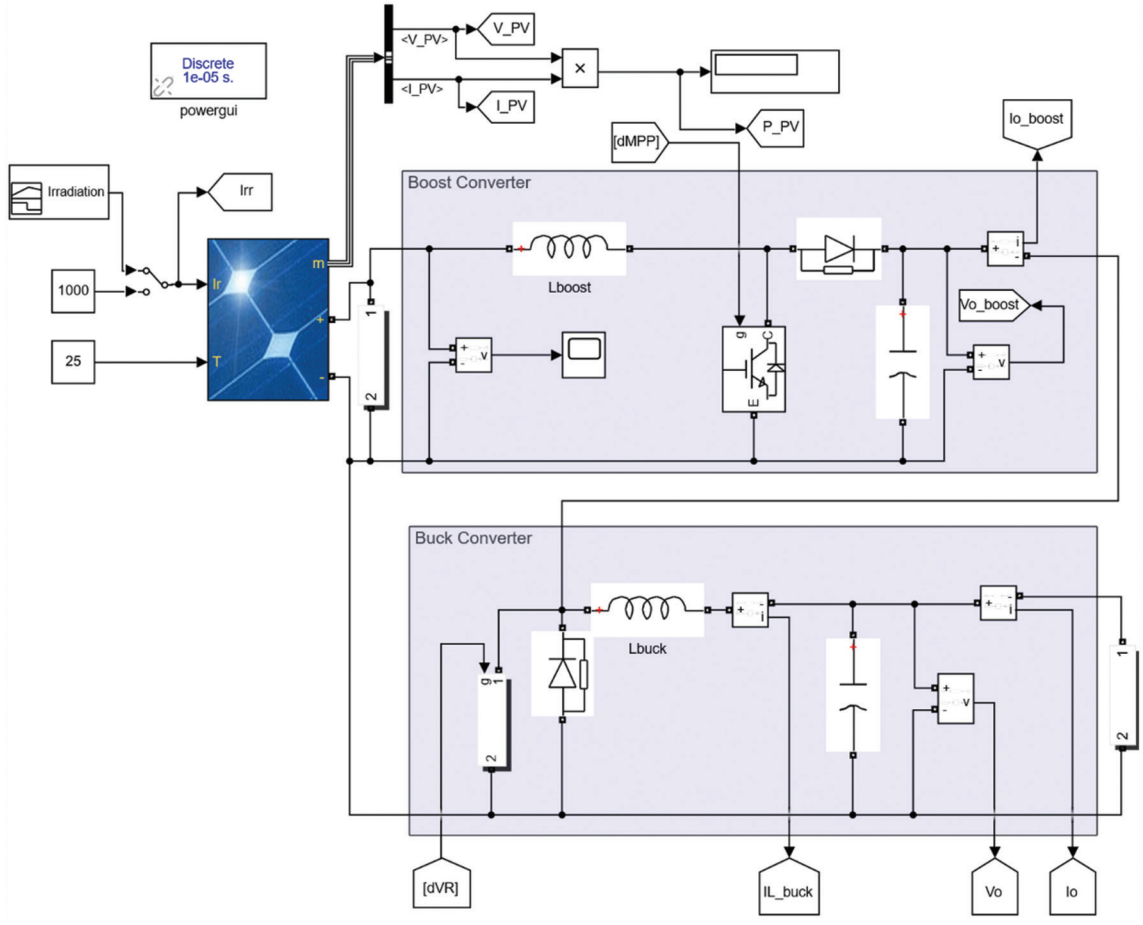

Fig. 8. Simulink model of the photovoltaic system (solar panel and DC–DC converters).

If $\sigma < 0$, then $u = 1$. From Eq. (19), in order for $\dot{\sigma} > 0$ to be satisfied, the output voltage has to be positive (i.e. $x_2 > 0$). Similarly, if a $\sigma > 0$, then $u = 0$. In order for $\dot{\sigma} < 0$ to be satisfied, the output voltage has to be less than the input voltage (i.e. $x_2 < v_{in}$). In other words, the reaching condition will be fulfilled as long as the condition ($0 < x_2 < v_{in}$) is satisfied. In the case of a buck converter, this condition is inherently accomplished. Therefore, it can be concluded that applying the presented control law, the stability of the system will be achieved (Guldemir, 2015). The strategy implemented to regulate the voltage of the photovoltaic system is summarised in Figure 7.

5. Results and Discussions

In this section, the results obtained for both the MPPT and voltage regulation of the PV system are presented. The simulations were performed using the Specialized Power Systems library of MATLAB/Simulink software. The photovoltaic system and controller models are shown in Figures 8 and 9, respectively. The main characteristics under STC of the chosen PV module are shown in Table 1. The parameters of the converters used for MPPT and voltage regulation of the PV system are presented in Table 2.

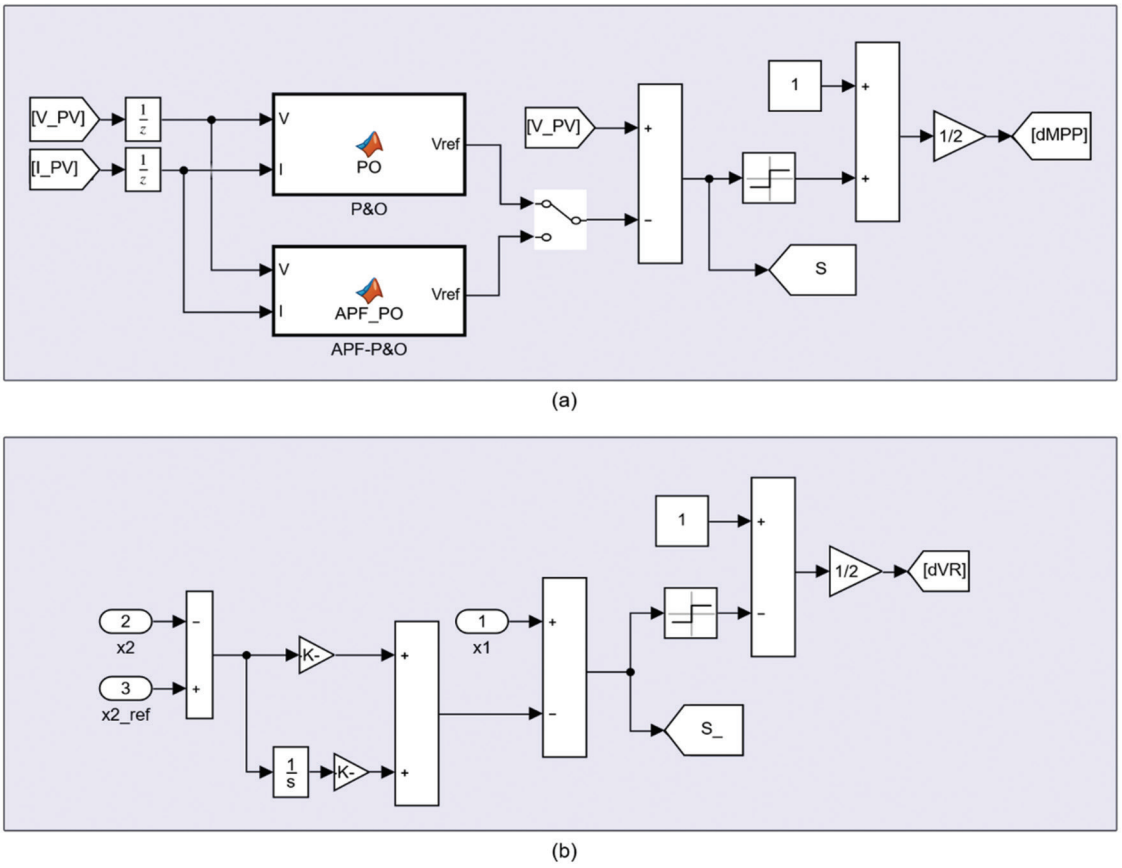

Fig. 9. Controllers implemented in MATLAB/Simulink software: (a) for MPPT and (b) for voltage regulation. APF, artificial potential fields; MPPT, maximum power point tracking; P&O, perturb and observe.

Cells	
Technology	Polycrystalline silicon
Number of cells	66
Dimensions	156 mm × 156 mm
Structural characteristics	
Dimensions L × W × H	1,803 mm × 995 mm × 50 mm
Weight	22.0 kg
Electrical characteristics	
Maximum power *Pmax*	250 W
Open circuit voltage *Voc*	40.06 V
Max. power point voltage *Vmpp*	33.40 V
Short-circuit current *Isc*	8.10 A
Max. power point current *Impp*	7.49 A

STC, standard test conditions.

Table 1. Key features of the TynSolar TYN-250P6 module under STC.

Boost converter design parameters	
Input capacitance (*C*)	4 μF
Inductance (*L*)	4.6 mH
Output capacitance (*C*)	181.85 μF
Switching frequency (*fsw*)	10 kHz
Buck converter design parameters	
Inductance (*L*)	100 mH
Capacitance (*C*)	10 μF
Load (*R*)	60 Ω
Switching frequency (*fsw*)	10 kHz

Table 2. Parameters of the DC–DC converters.

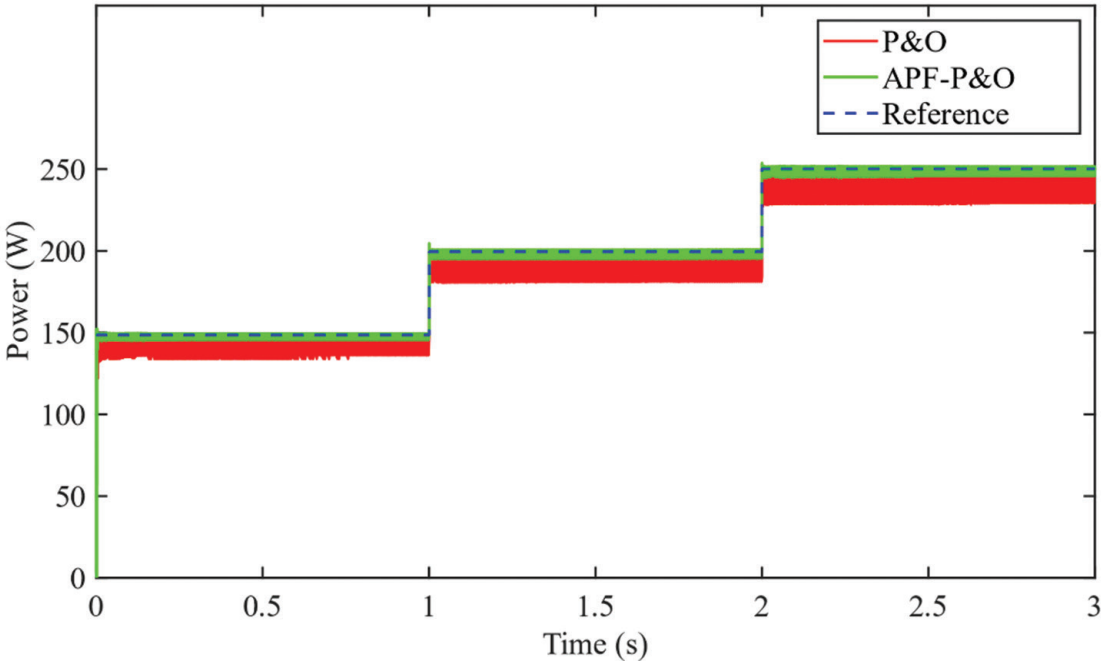

Fig. 10. Comparison between the presented APF-P&O method and the conventional P&O. APF, artificial potential fields; P&O, perturb and observe.

5.1. Simulation results for MPPT

The performance of the proposed APF-P&O algorithm is evaluated under different solar irradiation conditions, and then, comparisons are made with the conventional P&O method. In Figure 10, the results obtained for MPPT are presented, where the solar irradiation is 600 W/m^2, from 0 s to 1 s; then, it reaches 800 W/m^2 from 1 s to 2 s and 1,000 W/m^2 from 2 s to 3 s. Figure 11 is a zoomed-in version of Figure 10 highlighting the ripples in the output power of each method. Table 3 shows the efficiencies obtained for each method. The tracking efficiency used to compare the performance of the methods is defined as in Bendib et al. (2015). As can be clearly seen from the results, the implemented APF-P&O method presents a better performance compared to the conventional P&O method.

5.2. Simulation results for voltage regulation

Under the same solar irradiation conditions, the voltage regulation results are obtained. The reference voltage is assumed to be 32 V. The output voltage responses of the boost and buck converters are illustrated in Figures 12 and 13, respectively. The results show that although the input voltage of the buck converter varies due to changes in solar irradiation, its output voltage remains regulated.

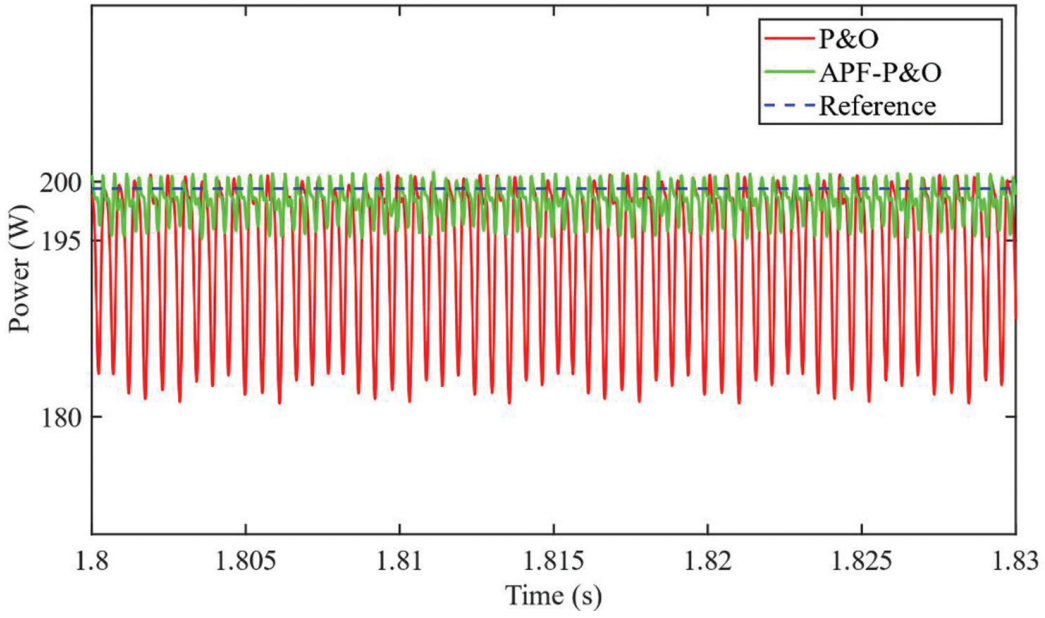

Fig. 11. Zoomed-in version of Figure 10 showing the magnitude of ripple in the output power. APF, artificial potential fields; P&O, perturb and observe.

MPPT algorithm	Efficiency (%)
P&O	96.4
APF-P&O	99.5

APF, artificial potential fields; MPPT, maximum power point tracking; P&O, perturb and observe.

Table 3. Comparison of tracking efficiency.

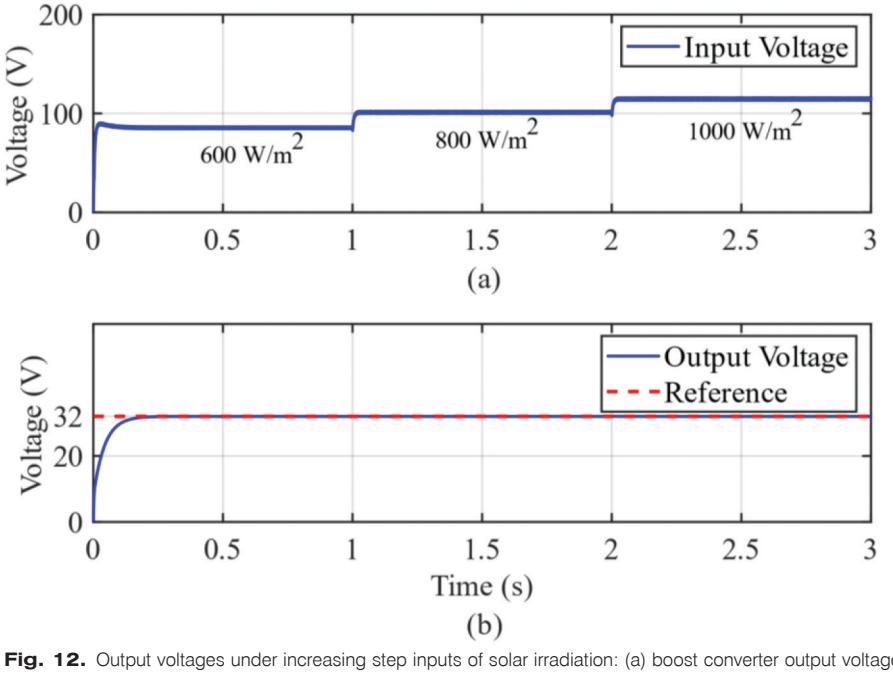

Fig. 12. Output voltages under increasing step inputs of solar irradiation: (a) boost converter output voltage and (b) buck converter output voltage (or PV system output voltage).

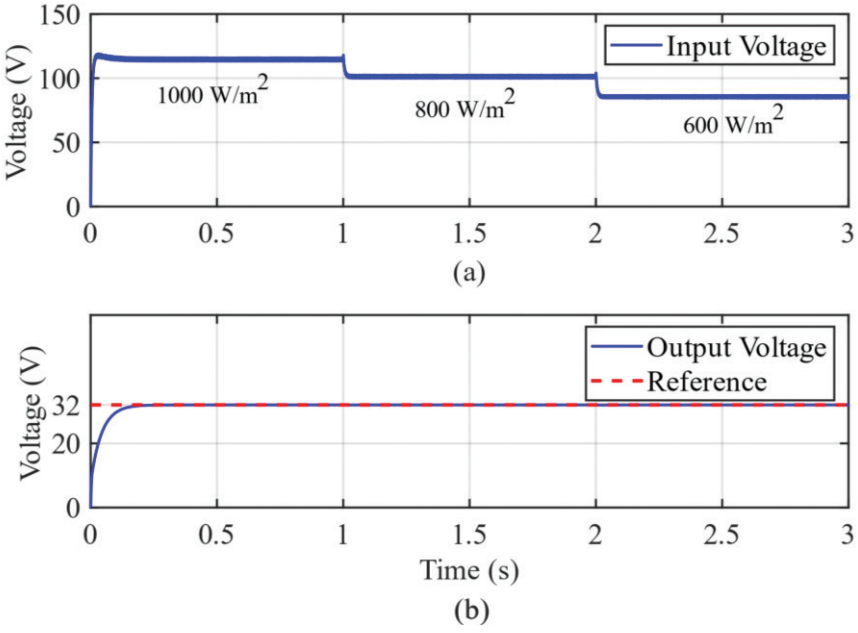

Fig. 13. Output voltages under decreasing step inputs of solar irradiation: (a) boost converter output voltage and (b) buck converter output voltage (or PV system output voltage).

6. Conclusion

This study presented a control strategy where both maximum power tracking and voltage regulation of a PV system are achieved simultaneously. A method for MPPT inspired by APF called APF-P&O is presented, and by means of comparisons with the conventional P&O method, its effectiveness is proven. The voltage obtained by the MPPT method is sent to the SMC which commands the boost input so that the MPP is reached. According to the simulations, the implemented APF-P&O method presents a relatively better performance in terms of efficiency, and output power ripples. For voltage regulation, another SMC with an appropriate control law is employed. Through simulations, it is verified that regardless of the variation of solar irradiation and the input voltage of the buck converter, the output voltage of the PV system remains regulated at the desired value. All simulations were performed using MATLAB/Simulink software. A recommendation for future research would be to add an anti-drifting feature to the implemented APF-P&O method.

References

Ali, M. N., Mahmoud, K., Lehtonen, M. and Darwish, M. M. F. (2021). An Efficient Fuzzy-Logic Based Variable-Step Incremental Conductance MPPT Method for Grid-Connected PV Systems. *IEEE Access*, 9, pp. 26420–26430. doi: 10.1109/ACCESS.2021.3058052.

Altamimi, S. N., Feilat, E. A. and Al Nadi, D. A. (2021). Maximum Power Point Tracking Technique Using Combined Incremental Conductance and Owl Search Algorithm. In: *2021 12th International Renewable Engineering Conference (IREC)*. IEEE, pp. 1–6. doi: 10.1109/IREC51415.2021.9427812.

Benadli, R., Bjaoui, M., Khiari, B. and Sellami, A. (2021). Sliding Mode Control of Hybrid Renewable Energy System Operating in Grid Connected and Stand-Alone Mode. *Power Electronics and Drives*, 6(1), pp. 144–166. doi: 10.2478/pead-2021-0009.

Bendib, B., Belmili, H. and Krim, F. (2015). A Survey of the Most Used MPPT Methods: Conventional and Advanced Algorithms Applied for Photovoltaic Systems. *Renewable and Sustainable Energy Reviews*, 45(May), pp. 637–648. doi: 10.1016/j.rser.2015.02.009.

Chowdhury, S. B. R., Mukherjee, A. and Gayen, P. K. (2021). Maximum Power Point Tracking of Photovoltaic System by Perturb & Observe and Incremental Conductance Methods Under Normal and Partial Shading Conditions. In: *2021 Innovations in Energy Management and Renewable Resources (52042)*. IEEE, pp. 1–6. doi: 10.1109/IEMRE52042.2021.9386964.

Elahi, M., Ashraf, H. M. and Kim, C.-H. (2022). An Improved Partial Shading Detection Strategy Based on Chimp Optimization Algorithm to Find Global Maximum Power Point of Solar Array System. *Energies*, 15(4), p. 1549. doi: 10.3390/en15041549.

Farhat, M., Barambones, O. and Sbita, L. (2017). A New Maximum Power Point Method Based on a Sliding Mode Approach for Solar Energy Harvesting. *Applied Energy*, 185, pp. 1185–1198. doi: 10.1016/j.apenergy.2016.03.055.

Goudarzian, A., Khosravi, A. and Raeisi, H. A. (2019). Optimized Sliding Mode Current Controller for Power Converters with Non-Minimum Phase Nature. *Journal of the Franklin Institute*, 356(15), pp. 8569–8594. doi: 10.1016/j.jfranklin.2019.08.026.

Grzesiak, L. (2017). Hybrid MPPT Algorithm for PV Systems Under Partially Shaded Conditions Using a Stochastic Evolutionary Search and a Deterministic Hill Climbing. *Power Electronics and Drives*, 2(2), pp. 49–59. doi: 10.5277/PED170212.

Guldemir, H. (2015). Study of Sliding Mode Control of DC–DC Buck Converter. (January 2011). doi: 10.4236/epe.2011.34051.

Inomoto, R. S., Monteiro, J. R. B. A. and Sguarezi Filho, A. J. (2022). Boost Converter Control of PV System Using Sliding Mode Control With Integrative Sliding Surface. *IEEE Journal of Emerging and Selected Topics in Power Electronics*, 6777(c), pp. 1–1. doi: 10.1109/jestpe.2022.3158247.

Jayaprakash, S. and Ramakrishnan, V. (2014). Analysis of Solar Based Closed Loop DC–DC Converter Using PID and Fuzzy Logic Control for Separately Excited Motor Drive. In: *2014 IEEE National Conference on Emerging Trends In Renewable Energy Sources And Energy Management (NCET NRES EM)*, pp. 118–122. doi: 10.1109/NCETNRESEM.2014.708875.

Kermadi, M., Salam, Z., Eltamaly, A. M., Ahmed, J., Mekhilef, S., Larbes, C. and Berkouk, E. M. (2020). Recent Developments of MPPT Techniques for PV Systems Under Partial Shading Conditions: A Critical Review and Performance Evaluation. *IET Renewable Power Generation*, 14(17), pp. 3401–3417.

Kesilmiş, Z. (2022). A Manhattan Metric Based Perturb and Observe Maximum Power Point Tracking Algorithm for Photovoltaic Systems. *Energy Sources, Part A: Recovery, Utilization, and Environmental Effects*, 44(1), pp. 469–492. doi: 10.1080/15567036.2022.2046662.

Komurcugil, H., Biricik, S., Bayhan, S. and Zhang, Z. (2021). Sliding Mode Control: Overview of Its Applications in Power Converters. *IEEE Industrial Electronics Magazine*, 15(1), pp. 40–49. doi: 10.1109/MIE.2020.2986165.

Kordestani, M., Mirzaee, A., Safavi, A. A. and Saif, M. (2018). Maximum Power Point Tracker (MPPT) for Photovoltaic Power Systems – A Systematic Literature Review. In: *2018 European Control Conference (ECC)*. IEEE, pp. 40–45. doi: 10.23919/ECC.2018.8550117.

Ling, R., Shu, Z., Hu, Q. and Song, Y.-D. (2018). Second-Order Sliding-Mode Controlled Three-Level Buck DC–DC Converters. *IEEE Transactions on Industrial Electronics*, 65(1), pp. 898–906. doi: 10.1109/TIE.2017.2750610.

Ma, M., Liu, X. and Lee, K. Y. (2020). Maximum Power Point Tracking and Voltage Regulation of Two-Stage Grid-Tied PV System Based on Model Predictive Control. *Energies*, 13(6), p. 1304. doi: 10.3390/en13061304.

Manuel, N. L., İnanç, N. and Erten, M. Y. (2021). Control of Mobile Robot Formations Using A-star Algorithm and Artificial Potential Fields. *Journal of Mechatronics, Electrical Power, and Vehicular Technology*, 12(2), pp. 57–67. doi: 10.14203/j.mev.2021.v12.57-67.

Mira, M. C., Knott, A., Thomson, O. C. and Andersen, M. A. E. (2013). Boost Converter with Combined Control Loop for A Stand-Alone Photovoltaic Battery Charge System. In: *2013 IEEE 14th Workshop on Control and Modeling for Power Electronics (COMPEL)*. IEEE, pp. 1–8. doi: 10.1109/COMPEL.2013.6626428.

Mohamed, S. A. and Abd El Sattar, M. (2019). A Comparative Study of P&O and INC Maximum Power Point Tracking Techniques for Grid-Connected PV Systems. *SN Applied Sciences*, 1(2), p. 174. doi: 10.1007/s42452-018-0134-4.

Park, H.-H. and Cho, G.-H. (2014). A DC–DC Converter for a Fully Integrated PID Compensator with a Single Capacitor. *IEEE Transactions on Circuits and Systems II: Express Briefs*, 61(8), pp. 629–633. doi: 10.1109/TCSII.2014.2327351.

Podder, A. K., Roy, N. K. and Pota, H. R. (2019). MPPT Methods for Solar PV Systems: A Critical Review Based on Tracking Nature. *IET Renewable Power Generation*, 13(10), pp. 1615–1632.

Pradhan, C., Senapati, M. K., Ntiakoh, N. K. and Calay, R. K. (2022). Roach Infestation Optimization MPPT Algorithm for Solar Photovoltaic System. *Electronics*, 11(6), p. 927. doi: 10.3390/electronics11060927.

Rahman Habib, H. U., Wang, S., Elmorshedy, M. F. and Waqar, A. (2019). Performance Analysis of Combined Model-Predictive and Slide-Mode Control for Power Converters in Renewable Energy Systems. In: *2019 22nd International Conference on Electrical Machines and Systems (ICEMS)*. IEEE, pp. 1–5. doi: 10.1109/ICEMS.2019.8921860.

Ravindranath Tagore, Y., Rajani, K. and Anuradha, K. (2022). Dynamic Analysis of Solar Powered Two-Stage DC–DC Converter with MPPT and Voltage Regulation. *International Journal of Dynamics and Control*, pp. 1–15. doi: 10.1007/s40435-022-00930-8.

Saidi, A. and Benachaiba, C. (2016). Comparison of IC and P&O Algorithms in MPPT for Grid Connected PV Module. In: *2016 8th International Conference on Modelling, Identification and Control (ICMIC)*. IEEE, pp. 213–218. doi: 10.1109/ICMIC.2016.7804300.

Saidi, K., Maamoun, M. and Bounekhla, M. (2019). A New High Performance Variable Step Size Perturb-and-Observe MPPT Algorithm for Photovoltaic System. *International Journal of Power Electronics and Drive Systems (IJPEDS)*, 10(3), p. 1662. doi: 10.11591/ijpeds.v10.i3.pp1662-1674.

Sarvi, M. and Azadian, A. (2021). A Comprehensive Review and Classified Comparison of MPPT Algorithms in PV Systems. *Energy Systems*, 13(2), pp. 281–320. doi: 10.1007/s12667-021-00427-x

Sheikh Ahmadi, S. H., Karami, M., Gholami, M. and Mirzaei, R. (2022). Improving MPPT Performance in PV Systems Based on Integrating the Incremental Conductance and Particle Swarm Optimization Methods. *Iranian Journal of Science and Technology, Transactions of Electrical Engineering*, 46(1), pp. 27–39. doi: 10.1007/s40998-021-00459-0.

Stephen, A. A., Musasa, K. and Davidson, I. E. (2022). Modelling of Solar PV Under Varying Condition with an Improved Incremental Conductance and Integral Regulator. *Energies*, 15(7), p. 2405. doi: 10.3390/en15072405.

Sulligoi, G., Bosich, D., Giadrossi, G., Zhu, L., Cupelli, M. and Monti, A. (2014). Multiconverter Medium Voltage DC Power Systems on Ships: Constant-Power Loads Instability Solution Using Linearization via State Feedback Control. *IEEE Transactions on Smart Grid*, 5(5), pp. 2543–2552. doi: 10.1109/TSG.2014.2305904.

Ullah, S. (2021). Robust Back-stepping Based Higher Order Sliding Mode Control of Non-Inverted Buck-Boost Converter for a Photovoltaic System. *Power Electronics and Drives*, 6(1), pp. 113–127. doi: 10.2478/pead-2021-0007.

Utkin, V. (2013). Sliding Mode Control of DC/DC Converters. *Journal of the Franklin Institute*, 350(8), pp. 2146–2165. doi: 10.1016/j.jfranklin.2013.02.026.

Wei, Q. et al. (2017). Model Predictive Control of Capacitor Voltage Balancing for Cascaded Modular DC–DC Converters. *IEEE Transactions on Power Electronics*, 32(1), pp. 752–761. doi: 10.1109/TPEL.2016.2530869.

Wu, L., Wu, B., Xu, D. and Zargari, N. R. (2022). Sliding Mode Control in Power Converters and Drives: A Review. *IEEE/CAA Journal of Automatica Sinica*, 9(3), pp. 392–406. doi: 10.1109/JAS.2021.1004380.

Xu, Z.-R., Yang, P., Zhou, D.-B., Li, P., Lei, J.-Y. and Chen, Y.-R. (2015). An Improved Variable Step Size MPPT Algorithm Based on INC. *Journal of Power Electronics*, 15(2), pp. 487–496. doi: 10.6113/JPE.2015.15.2.487.